Volume 3, Number 3, 2026

Pages 1075-1094

Bioscience Insights

ISSN: 3080-3489 (Print)
ISSN: 3080-3497 (Online)

BiosciInsights.com

MAGNETICALLY FUNCTIONALIZED $NiFe_2O_4$–DECORATED DALBERGIA SISSOO BIOCHAR NANOCOMPOSITE FOR THE EFFICIENT 4–NITROPHENOL REMEDIATION

Muhammad Imran[1*], Dr. Humaira Khan[2*], Dr. Aamna Balouch[3], Farooq Azam[4]

[*1,2,4] *Department of Chemistry, M.A. Kazi Institute of Chemistry, University of Sindh, Jamshoro, Sindh, Pakistan*
[3] *National Centre of Excellence in Analytical Chemistry, University of Sindh, Jamshoro, Sindh, Pakistan*

https://doi.org/10.5281/zenodo.23794783

Article Information

Article History

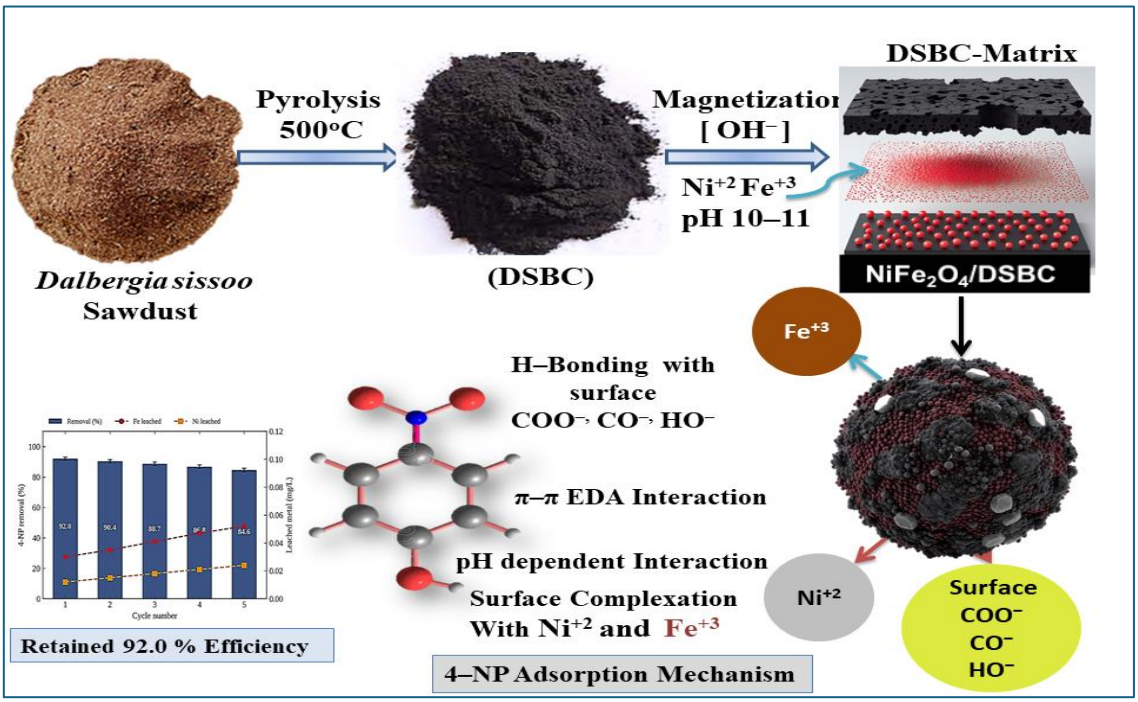
Received:	June 19, 2026
Revised:	August 19, 2026
Accepted:	September 07, 2026
Available Online:	October 30, 2026

Keywords:
Magnetic Biochar, Nickel ferrite, Dalbergia sissoo, 4-nitrophenol, Adsorption, Magnetic separation

Abstract

Sawdust of Dalbergia sissoo was pyrolyzed to biochar (DSBC) and used as a support for nickel ferrite ($NiFe_2O_4$) to prepare a magnetically separable adsorbent for 4-nitrophenol (4-NP). The $NiFe_2O_4$/DSBC composite had a BET surface area of 148.6 m^2/g, a mean crystallite size of 21.4 nm and a saturation magnetization of 8.67 emu/g. Under the selected conditions (pH 5.0, adsorbent dose 1.0 g/L, initial concentration 50 mg/L, 180 min and 298 K), 4-NP removal reached 92.0% (46.0 mg/g). The kinetic data followed the pseudo-second-order model ($q_{e,cal}$ = 46.7 mg/g, k_2 = 0.0032 g mg^{-1} min^{-1}, R^2 = 0.997), and the equilibrium data were best described by the Langmuir isotherm, with maximum capacities of 85.0, 92.0 and 99.0 mg/g at 298, 308 and 318 K, respectively. Thermodynamic analysis indicated a spontaneous and endothermic process ($\Delta H°$ = 18.5 kJ/mol; $\Delta S°$ = 75.0 J mol^{-1} K^{-1}). After five adsorption–desorption cycles, removal remained at 84.6%, corresponding to 92.0% retention of the first-cycle efficiency. These results show that $NiFe_2O_4$/DSBC is a promising, magnetically recoverable adsorbent for nitrophenol-contaminated water.

GRAPHICAL ABSTRACT



1. INTRODUCTION

Nitro phenol is a class of nitroaromatic compounds that are contaminant of surface and ground water sources due to the effluents from pesticide, dye, explosive, pharmaceutical and leather industries. Of these, 4-nitrophenol (4-NP) is of special concern due to its toxicity, slow biodegradation in the environment and chemical stability [1]. Nitrophenols are listed as priority pollutants by the U.S. Environmental Protection Agency and have ambient water quality criteria published by the EPA (U.S. Environmental Protection Agency [EPA], 1980). Thus, it is essential to remove them from industrial effluents before they are discharged into water, to safeguard both aquatic ecosystems and drinking-water sources.

Water treated with nitrophenols can be treated by several methods such as chemical oxidation, photocatalysis, biological degradation, membrane processes and adsorption. Adsorption is the process generally preferred due to its ease of operation, versatility on effluent composition and because no harmful byproducts are produced if the adsorbent is used properly [2]. Commercial activated carbon can be used as an effective adsorbent, but its high cost and regeneration requirements make it unsuitable for use in low-income areas and has stimulated the development of carbonaceous adsorbents from agricultural and forestry residues.

Biochar is a carbon-rich solid that is produced during a pyrolysis process which occurs under limited oxygen conditions [3]. It is aromatic carbon skeleton, porous structure, has functional groups on its surface that are capable of binding organic and inorganic contaminants and in general is cheaper than activated carbon [4-6]. The surface area, ash content, aromaticity and surface chemistry of the product strongly depend on the feedstock and pyrolysis conditions, which in turn influences the sorption performance of the product [7]. *Dalbergia sissoo* (Shisham) is one of the commonly seen timber trees in Pakistan and the entire Indian subcontinent and sawmill industries produce huge amount of sawdust that is either burnt or discarded. Purification of dyes using wood dust and leaf powder of D. sissoo has already been investigated as a suitable adsorbent [8, 9], but the use of D. sissoo as a biochar support for a magnetic nanocomposite for removal of nitrophenols has been largely overlooked.

Another practical problem with powdered biochar is its inability to be separated from treated water, whether it is filtered or settled. When the biochar is used in combination with magnetic phases, it can

be recovered quickly by using an external magnet and can provide new adsorption sites [10, 11]. Nickel Ferrite $NiFe_2O_4$ is a ferrimagnetic ferrite with excellent chemical stability, suitable for magnetic component use. The use of carbon–$NiFe_2O_4$ composite prepared using sawdust for nitroaromatic compounds [12] means that it is possible to use a wood-derived carbon in combination with nickel ferrite.

In this work, $NiFe_2O_4$/DSBC nanocomposite was synthesized using the co-precipitation method by using the biochar prepared from D. sissoo sawdust as support. The goals of this study were (a) characterization of structure, morphology, porosity and magnetic behavior of the composite, (b) study of its efficiency in the removal of 4-NP as a function of pH, dose, contact time, initial concentration and temperature, (c) interpretation of the process through kinetic, isotherm and thermodynamic models, and (d) assessment of the reusability and magnetic recovery of the adsorbent.

2. Materials and Methods

2.1 Chemicals

Nickel (II) nitrate hexahydrate ($Ni(NO_3)_2{\cdot}6H_2O$), Iron (III) nitrate nonahydrate ($Fe(NO_3)_3{\cdot}9H_2O$), sodium hydroxide (NaOH), hydrochloric acid (HCl), ethanol and 4-nitrophenol (≥99%) were of analytical grade and used as received. De-ionized (DI) water was used throughout. A 4-NP stock solution (1000 mg/L) was prepared in DI water and diluted as required.

2.2 Preparation of Biochar from Dalbergia sissoo Sawdust

The sawdust of Dalbergia sissoo was obtained from a local saw mill in city, Pakistan. It was repeatedly washed with DI water to wash off dust and soluble contaminants, dried in an oven at 80 °C for 24 h and sieved to remove coarse particles. The dried sawdust was pyrolyzed in a tubular furnace at 500 °C for 2 h (heating rate 10 °C/min) under a continuous nitrogen flow (100 mL/min). The biochar was ground, sieved to <150 µm, washed with DI water until neutral (pH 7), dried at 80 °C and kept in desiccator (Figure 1). The product obtained is called *Dalbergia sissoo* Sawdust biochar (DSBC).

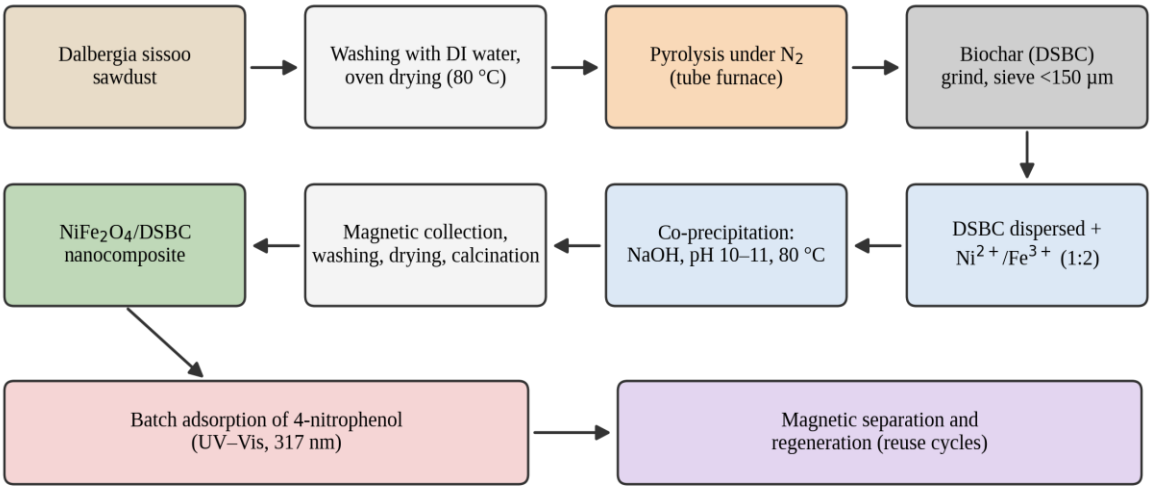


Figure 1 Preparation Route of the $NiFe_2O_4$/DSBC Nanocomposite and Its Application for 4-Nitrophenol Removal; (DSBC = Dalbergia Sissoo biochar; DI = deionized.)

2.3 Synthesis of the $NiFe_2O_4$/DSBC Nanocomposite

Co-precipitation was used to prepare nanocomposite. $Ni(NO_3)_2{\cdot}6H_2O$ (1.454 g, 5 mmol) and $Fe(NO_3)_3{\cdot}9H_2O$ (4.040 g, 10 mmol) (Ni:Fe molar ratio 1:2) were dissolved in 50 mL DI water and then added to the biochar suspension under strong stirring. The mixture was heated to 80 °C and the addition of 2 M NaOH solution was continued dropwise until the pH value was adjusted to 10–11. The stirring was continued for 2 h and the suspension was aged for 1 h. The solid was collected by using a

magnet, washed with DI water until pH 7 and ethanol, dried at 80 °C for 12 h and calcined at 450 °C in a nitrogen atmosphere for 2 h. The theoretical yield of $NiFe_2O_4$ from these mass quantities is approximately 1.17 g of $NiFe_2O_4$ producing an approximate mass ratio of biochar to ferrite of 1:1.

2.4 Characterization

XRD (Cu Kα, λ = 1.5406 Å and 2θ = 10°–80°) was used to identify the crystalline phases. The average crystallite size (D) was estimated using the Scherrer equation (Scherrer, 1918):

$$D = K\lambda / (\beta \cos \theta) \quad (1)$$

where K is the shape factor (0.9), λ is the X-ray wavelength, β is the full width at half maximum of the diffraction peak (radians) and θ is the Bragg angle. Surface functional groups were examined by FTIR spectroscopy in the range 4000–400 cm^{-1} using KBr pellets. Morphology and elemental composition were studied by SEM–EDX. Specific surface area, pore volume and pore size were determined from N_2 adsorption–desorption isotherms at 77 K using the Brunauer–Emmett–Teller (BET) method [13], and isotherm shapes were classified according to IUPAC recommendations[14]. Magnetic properties were measured at room temperature by VSM. The point of zero charge (pH_{pzc}) was determined by the pH drift method using 0.01 M NaCl solutions with initial pH values of 2–10.

2.5 Batch Adsorption Experiments

The batch experiments were conducted in 100 mL conical flasks having 50 mL of the 4-NP solution, shaken in an orbital shaker at 150 rpm at a controlled temperature. pH of the solution was adjusted by the addition of 0.1 M HCl or NaOH. The adsorbent was then separated using a magnet and the remaining 4-NP concentration was determined by UV–Vis spectrophotometry at its absorption maximum of 4-NP (about 317 nm in acidic and neutral solution) and at its absorption maximum of phenolate form (about 400 nm at alkaline pH) following a calibration curve. The removal efficiency (R, %) and the adsorption amount of time t (q_t, mg/g) and at equilibrium (q_e, mg/g) were calculated by:

$$R\ (\%) = [(C_0 - C_e) / C_0] \times 100 \quad (2)$$

$$q_e = (C_0 - C_e)\, V / m \quad (3)$$

where C_0 and C_e (mg/L) are the initial and equilibrium concentrations, V (L) is the solution volume and m (g) is the adsorbent mass. The experimental ranges are summarized in Table 1. All experiments were carried out in triplicate, and mean values with standard deviations are reported. Control experiments without adsorbent were run to account for any loss of 4-NP not caused by adsorption.

Table 1 Experimental Conditions of the Batch Adsorption Study. (Agitation speed was 150 rpm and solution volume (V) was 50 mL in all experiments.)

Parameter	Range studied	Fixed value in other experiments
Solution pH	2–10	5.0
Adsorbent dose (g/L)	0.2–2.0	1.0
Contact time (min)	5–180	180
Initial 4-NP concentration (mg/L)	10–100	50
Temperature (K)	298, 308, 318	298

2.6 Kinetic, Isotherm and Thermodynamic Models

Kinetic data were fitted to the pseudo-first-order [15], pseudo-second-order [16] and Weber–Morris intraparticle diffusion [17] models:

$$\ln(q_e - q_t) = \ln q_e - k_1 t \quad (4)$$

$$t / q_t = 1 / (k_2 q_e^2) + t / q_e \quad (5)$$

$$q_t = k_{id} t^{0.5} + C \quad (6)$$

where k_1 (min^{-1}), k_2 ($g\ mg^{-1}\ min^{-1}$) and k_{id} ($mg\ g^{-1}\ min^{-0.5}$) are the rate constants and C is a constant related to the boundary-layer thickness. Equilibrium data were analyzed using the Langmuir [18] and Freundlich [18] isotherms:

$$C_e / q_e = 1 / (K_L q_m) + C_e / q_m \quad (7)$$

$$q_e = K_F C_e^{1/n} \quad (8)$$

where q_m (mg/g) is the maximum monolayer capacity, K_L (L/mg) is the Langmuir constant, K_F ($(mg/g)(L/mg)^{1/n}$) is the Freundlich constant and n is the heterogeneity factor. Thermodynamic parameters were obtained from:

$$\Delta G^\circ = -RT \ln K_c \quad (9)$$

$$\ln K_c = \Delta S^\circ / R - \Delta H^\circ / (RT) \quad (10)$$

In the above expression, K_c is the dimensionless equilibrium constant, R is the gas constant (8.314 $J\ mol^{-1}\ K^{-1}$) and T is the absolute temperature (K). Model fitting was assessed based on the coefficient of determination (R^2) and the agreement between experimental and calculated q_e and the linear regression was supplemented by error analysis in accordance with the recommendations concerning the correct treatment of adsorption data [19, 20].

2.7 Regeneration and Reusability

The adsorption composite was recovered using a magnet and regenerated by washing with 0.1 M NaOH /ethanol and then DI water until neutral pH, and then dried at 80 °C. This regenerated material was used five times for adsorption/desorption under the same conditions. The Ni and Fe concentration in the treated water was assessed using AA spectrophotometry.

3. Results and Discussion

3.1 Characterization of the Adsorbents

3.1.1 XRD Analysis

The XRD pattern of the DSBC, $NiFe_2O_4$ and $NiFe_2O_4$/DSBC are presented in Figure 2. The XRD spectra of the DSBC shows a wide hump at 2θ around 22°–25°, which is characteristic of poorly ordered turbostratic carbon. The composite shows reflections at 2θ ≈ 30.3°, 35.7°, 43.4°, 57.4° and 63.0°, assigned to the (220), (311), (400), (511) and (440) planes of cubic spinel $NiFe_2O_4$ (JCPDS Card No. 10-0325 inset in Figure 2), together with the carbon hump, which confirms that the ferrite phase was formed on the biochar. Using Equation 1, the average crystallite size was calculated and was equal to 21.4 nm as an average value based on the (311) peak.

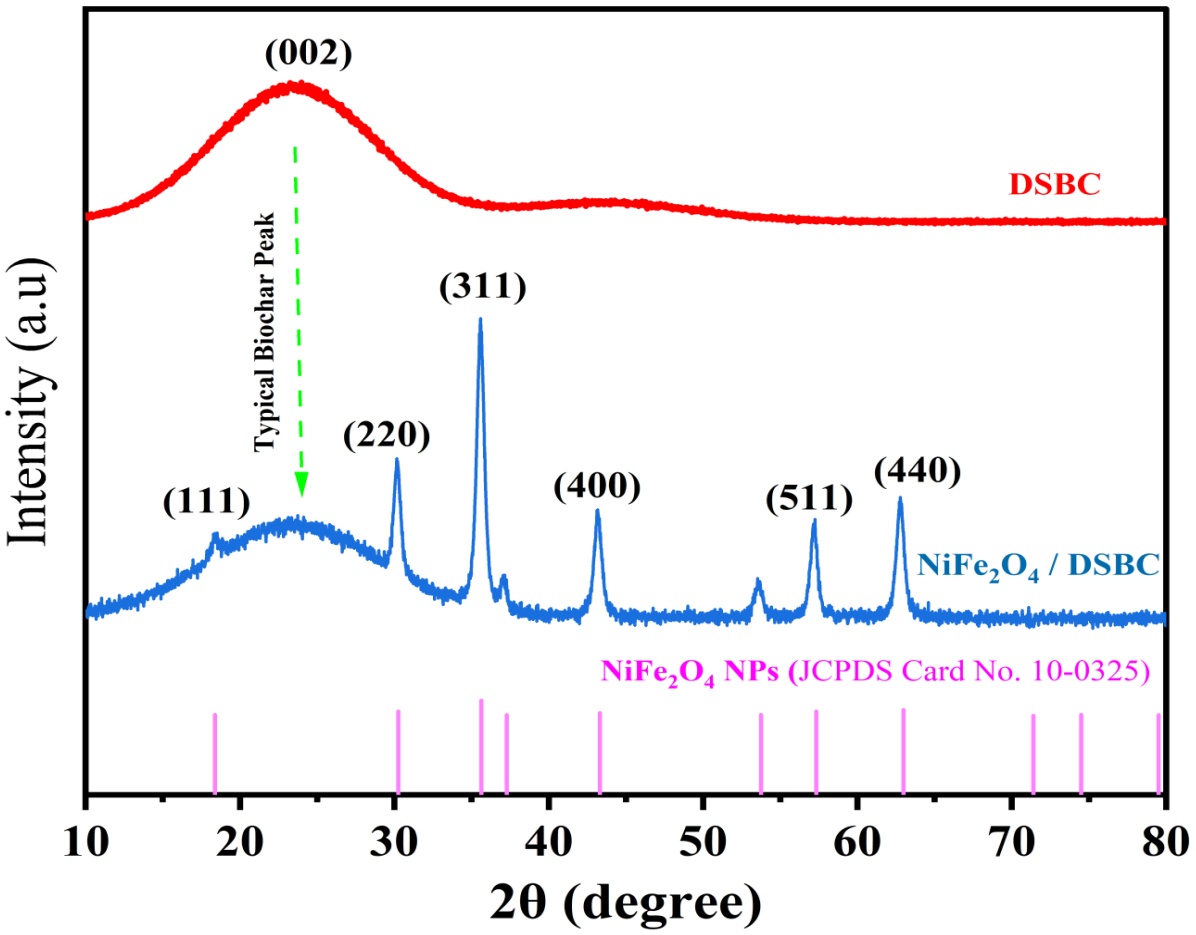


Figure 2 XRD Patterns of DSBC, $NiFe_2O_4$ and $NiFe_2O_4$/DSBC. ($NiFe_2O_4$; JCPDS Card No. 10-0325)

Note. JCPDS = Joint Committee on Powder Diffraction Standards.

3.1.2 FTIR Analysis

The FTIR spectra (Figure 3) of DSBC suggests the presence of oxygen containing groups on the biochar surface with bands near 3400 cm^{-1} (O–H stretching), 1700 cm^{-1} (C=O), 1600 cm^{-1} (aromatic C=C) and 1100 cm^{-1} (C–O). The metal–oxygen (Fe–O/Ni–O) stretching vibration in tetrahedral sites in the spinel lattice is identified as a strong band at ~580–600 cm^{-1} in the composite, while the shifts of the O–H and C=O bands suggest interaction between the ferrite and biochar functional groups. The presence of new or shifted bands near 1510 and 1340 cm^{-1} (asymmetric and symmetric NO_2 stretching indicated in pink shade Figure 3) after 4-NP adsorption provides proof for the surface retention of 4-NP.

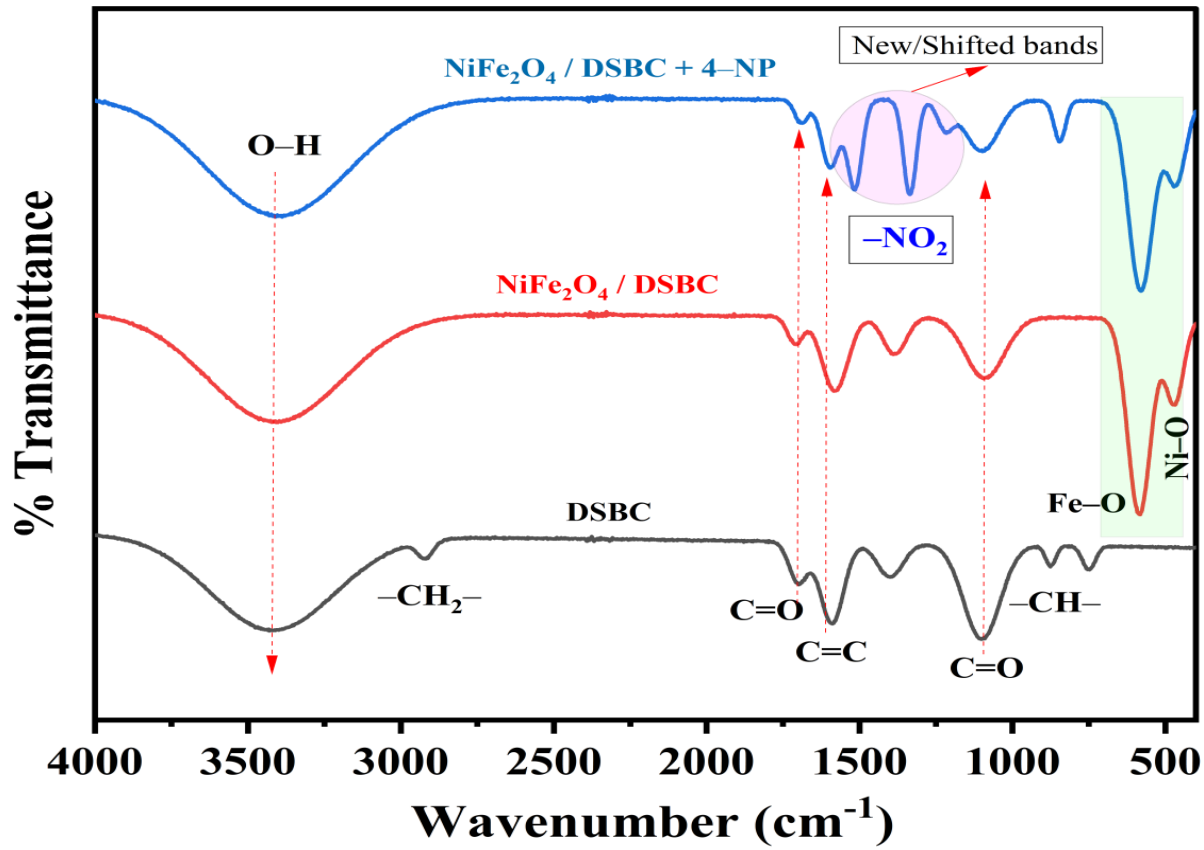


Figure 3 FTIR Spectra of DSBC, $NiFe_2O_4$/DSBC Before and After 4-Nitrophenol Adsorption

3.1.3 SEM–EDX Analysis

The SEM images (Figure 4) show the fibrous, porous structure of DSBC inherited from the wood cellular structure, and quasi-spherical $NiFe_2O_4$ particles of about 20–40 nm distributed on and within the biochar matrix with moderate agglomeration. EDX analysis of the composite detected C, O, Fe and Ni, with a Ni: Fe atomic ratio of about 1:2.03, in agreement with the intended spinel composition.

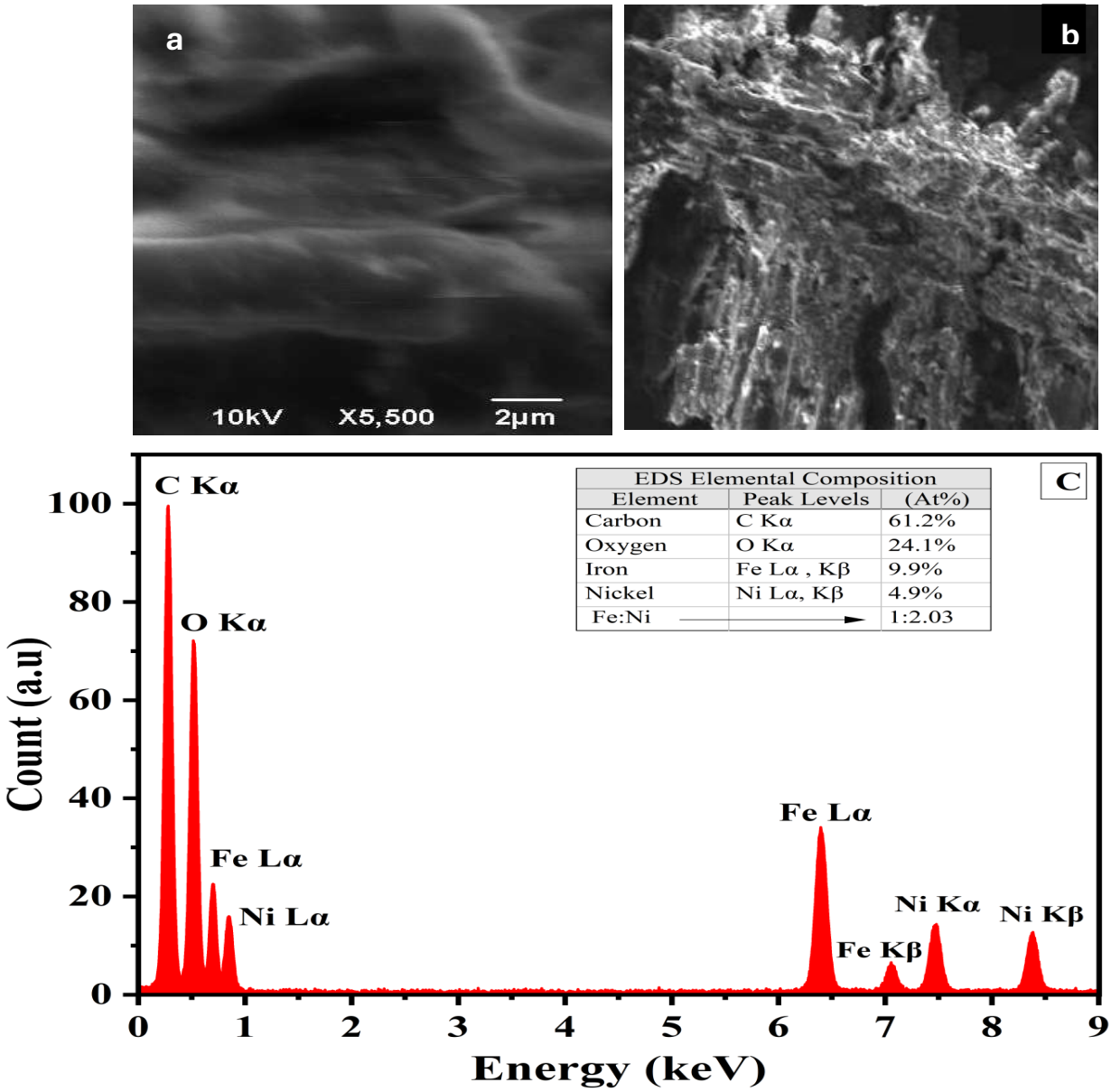


Figure 4 SEM Images and EDX Spectrum; Panels (a) and (b) show SEM images of DSBC and $NiFe_2O_4$/DSBC, respectively; panel (c) shows the EDX spectrum of the composite with the atomic composition as an inset.

3.1.4 Textural and Magnetic Properties

According to the IUPAC classification [14], the N_2 adsorption–desorption isotherms (Figure 5a) of the composite belong to the IV type with an H3 hysteresis loop, which suggests that the material has mesoporous properties. The BET surface area, pore volume and mean pore diameter are listed in Table 2. The surface area of the composite was 148.6 m^2/g, which is lower than that of DSBC (215.3 m^2/g) due to blocking of pore by ferrite particles. The VSM curves (Figure 5b) reveals a saturation magnetization of 8.67 emu/g for the composite, low coercivity and remanence are enough for rapid separation using a hand-held magnet.

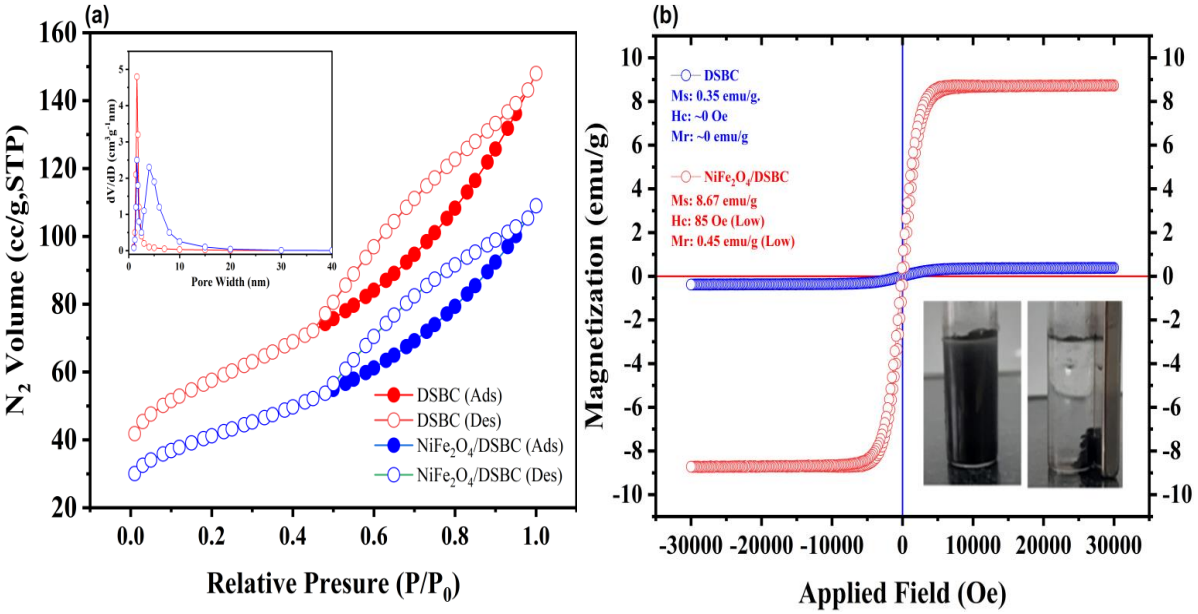


Figure 5 (a) N2 Adsorption–Desorption Isotherms with Pore-Size Distribution and (b) Magnetic Hysteresis Loops

Table 2 Physicochemical Characteristics of DSBC and $NiFe_2O_4$/DSBC

Property	DSBC	$NiFe_2O_4$/DSBC
BET surface area (m^2/g)	215.3	148.6
Total pore volume (cm^3/g)	0.162	0.145
Average pore diameter (nm)	3.01	3.90
Crystallite size (nm)	-	21.4
Saturation magnetization (emu/g)	~0	8.67
pH_{pzc}	5.8	6.4

Note. DSBC = Dalbergia sissoo biochar; pH_{pzc} = pH of point of zero charge.

3.2 Effect of Solution pH

The pK_a for 4-NP is approximately 7.15 and the pH of the solution affects both the surface charge of the adsorbent and the speciation of 4-NP. When the pH is less than this, 4-NP exists primarily in its neutral form, and when the pH is greater than this, it exists primarily in its negatively charged form (4-nitrophenolate ion). Removal was higher at pH 2 (61.0%) and reached a maximum of 92.0% at pH 5.0 and decreased at higher pH as shown in Figure 6. The value of pH_{pzc} for the composite was 6.4 (Table 2). The interaction between the negatively charged surface and the 4-NP is repulsive at pH values above the pH_{pzc} and the pK_a value of 4-NP, and at lower pH, the adsorption of the neutral molecule dominates. The same pH-dependent uptake of nitrophenol and other phenols was found with carbon-based sorbents [21]. Further experiments were then carried out at pH 5.0.

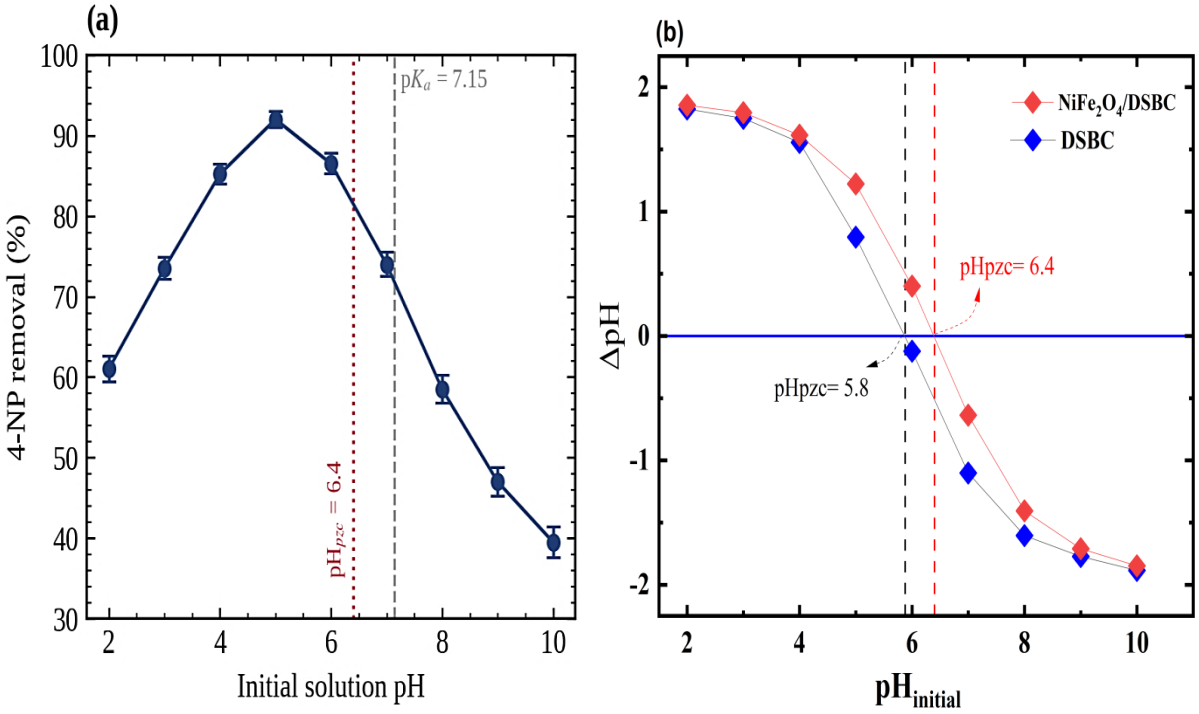


Figure 6: (a) Effect of Solution pH on 4-Nitrophenol Removal, and (b) Determination of pHpzc; Conditions: dose 1.0 g, time 180 min, initial concentration 50 mg/L, 298K

Note. Conditions: dose, initial concentration, time and temperature as in Table 1.

3.3 Effect of Adsorbent Dose

Increasing the dose from 0.2 to 2.0 g/L raised the removal efficiency from 34.0% to 98.0%, because more adsorption sites became available, while the adsorption capacity per unit mass decreased from 85.0 to 24.5 mg/g owing to unsaturation of sites at higher doses (Figure 7). A dose of 1.0 g/L was selected as a compromise between efficiency and material consumption.

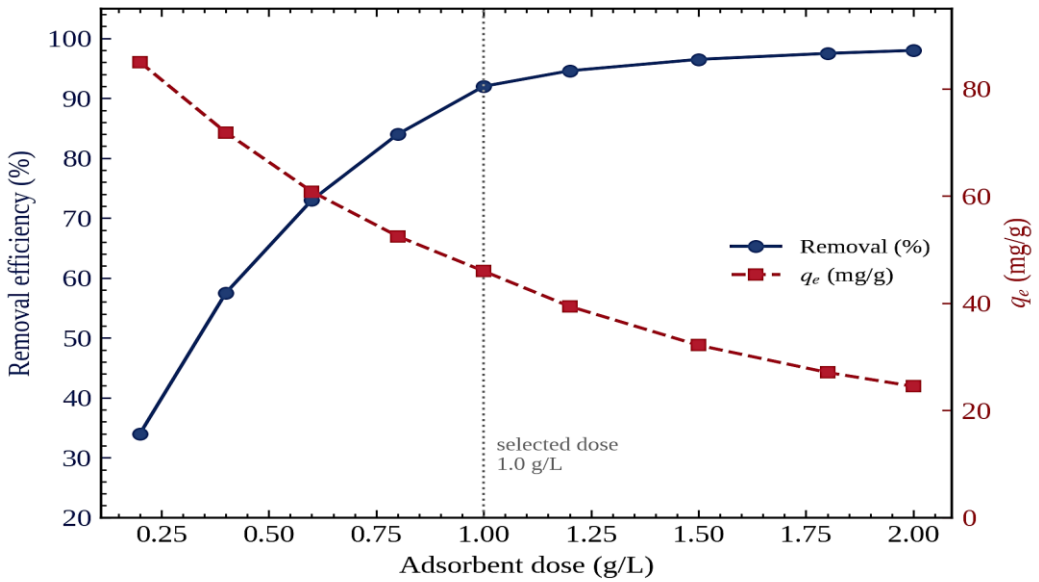


Figure 7 Effect of Adsorbent Dose on 4-Nitrophenol Removal Efficiency and Adsorption Capacity (Conditions: pH 5.0, C_0 = 50 mg/L, 180 min, 298 K)

3.4 Adsorption Kinetics

The effect of contact time is shown in Figure 8a. The adsorption process took place quickly for the first 30 min, due to the large amount of empty sites, and then slowed down until 180 min of adsorption when the equilibrium was reached. The corresponding kinetic parameters for the pseudo-first-order and pseudo-second-order models are shown in Table 3. The pseudo-second-order model showed the best R^2 (0.997) and the calculated q_e (46.7 mg/g) was the closest to the experimental q_e (46.0 mg/g), indicating that the rate was controlled by the surface interaction between 4-NP and the active sites [16]. Note that a good fit to the pseudo-second order equation does not necessarily indicate chemisorption [20]. The plot of Weber-Morris (Figure 8b) was not linear and not passing through the origin, suggesting the presence of intraparticle diffusion, but it is not the only rate limiting step.

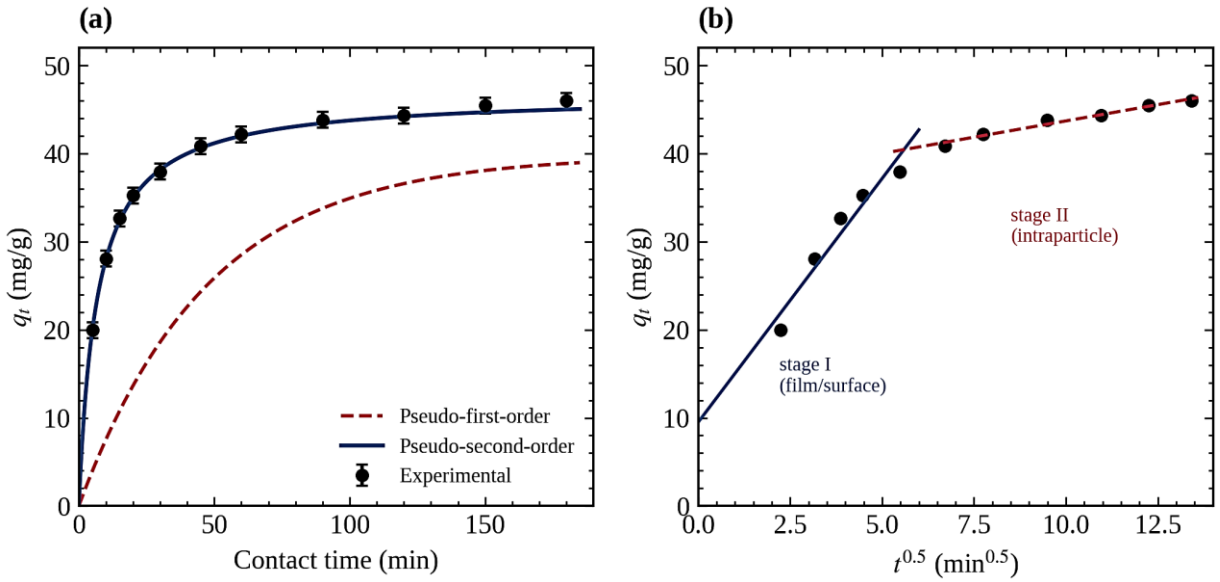


Figure 8 (a) Effect of Contact Time with Pseudo-First-Order and Pseudo-Second-Order Fits and (b) Weber–Morris Intraparticle Diffusion Plot

Note. Conditions: pH 5.0, dose 1.0 g/L, C_0 = 50 mg/L, 298 K.

Table 3 Kinetic Model Parameters for 4-Nitrophenol Adsorption onto $NiFe_2O_4$/DSBC

Model	Parameter	Value
Experimental	$q_{e,exp}$ (mg/g)	46.0
Pseudo-first-order	k_1 (min^{-1})	0.021
	$q_{e,cal}$ (mg/g)	39.8
	R^2	0.941
Pseudo-second-order	k_2 (g mg^{-1} min^{-1})	0.0032
	$q_{e,cal}$ (mg/g)	46.7
	R^2	0.997
Intraparticle diffusion	k_{id} (mg g^{-1} $min^{-0.5}$)	2.85
	C (mg/g)	11.2
	R^2	0.963

Note. Conditions as in Figure 8.

3.5 Adsorption Isotherms

Equilibrium data at 298, 308 and 318 K (Figure 9) were fitted to the Langmuir and Freundlich models, and the parameters are given in Table 4. The Langmuir model gave the higher R^2 at all temperatures (0.994–0.998), indicating monolayer coverage on a fairly homogeneous surface, and the maximum capacity was 85.0 mg/g at 298 K. The Freundlich exponent n of 2.4 (>1) points to favourable adsorption. The capacity of the composite relative to other adsorbents is considered in Section 4.3.

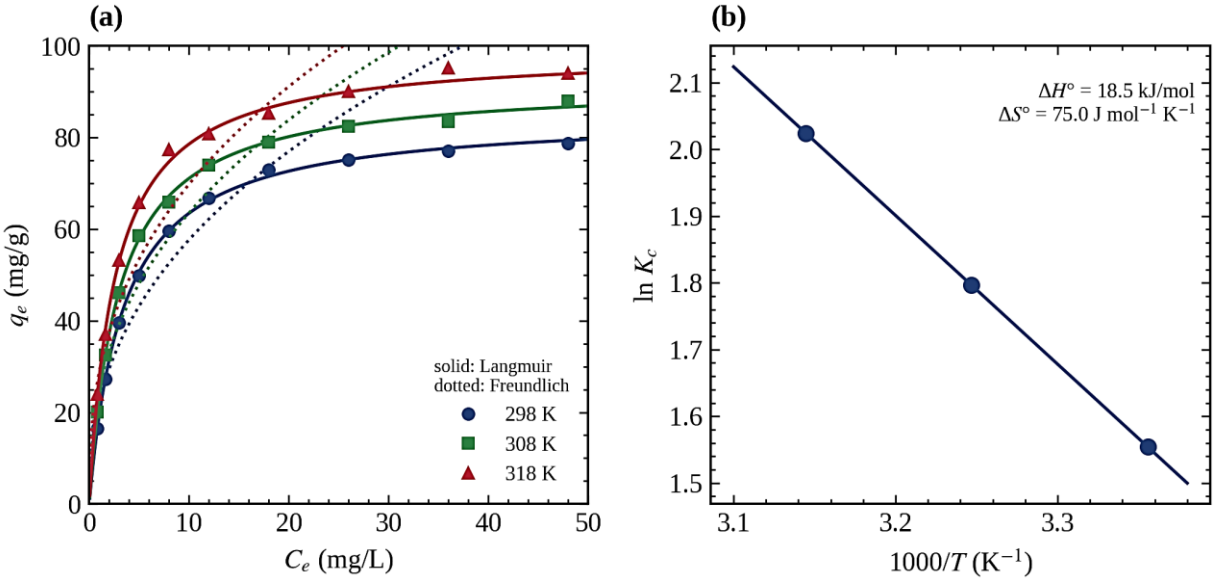


Figure 9 Adsorption Isotherms of 4-Nitrophenol onto $NiFe_2O_4$/DSBC at Different Temperatures: (a) Langmuir and Freundlich Fits and (b) van't Hoff Plot

Note. Conditions: pH 5.0, dose 1.0 g/L, 180 min.

Table 4 Isotherm Parameters for 4-Nitrophenol Adsorption onto $NiFe_2O_4$/DSBC

Isotherm	Parameter	298 K	308 K	318 K
Langmuir	q_m (mg/g)	85.0	92.0	99.0
	K_L (L/mg)	0.295	0.340	0.385
	R^2	0.994	0.996	0.998
Freundlich	K_F ((mg/g)(L/mg)$^{1/n}$)	22.1	25.3	28.8
	n	2.4	2.5	2.6
	R^2	0.961	0.968	0.973

Note. Conditions as in Figure 9.

3.6 Thermodynamic Study

The thermodynamic parameters are listed in Table 5. Negative ΔG° values at all temperatures confirm that the process is spontaneous, and the positive ΔH° (18.5 kJ/mol) indicates an endothermic process, which is consistent with the increase in capacity with temperature. The positive ΔS° (75.0 J mol^{-1} K^{-1}) reflects increased randomness at the solid–solution interface, probably because of displacement of water molecules from the surface during adsorption of 4-NP. These thermodynamic parameters alone do not establish the adsorption mechanism.

Table 5 Thermodynamic Parameters for 4-Nitrophenol Adsorption onto $NiFe_2O_4$/DSBC

T (K)	K_c	ΔG° (kJ/mol)	ΔH° (kJ/mol)	ΔS° (J/mol K)
298	4.73	-3.850	18.5	75.0
308	6.03	-4.600	18.5	75.0
318	7.57	-5.350	18.5	75.0

Note. ΔH° and ΔS° were obtained from the van't Hoff plot of ln K_c against 1/T.

3.7 Proposed Adsorption Mechanism

There can be multiple interactions between 4-NP and the $NiFe_2O_4$/DSBC composite (Figure 10). First, the electron-deficient nitro-substituted aromatic ring of 4-NP can interact with the electron-rich graphitic domains of biochar through π–π electron donor–acceptor (EDA) interactions, which has been proposed for nitro-aromatic compounds on biochars [22] .Second, both hydroxyl and nitro groups on 4-NP can hydrogen bond with the surface –OH and –COOH groups of the biochar and with the hydroxylated Fe/Ni sites on the surface of the ferrite, as indicated by the FTIR spectra (Section 3.1.2). Third, pore filling within the micropores and mesopores contributes additionally to uptake, while the pH dependence described in Section 3.2 indicates that electrostatic attraction or repulsion also affects the uptake of the ionized species. The relative importance of these interactions is discussed in Section 4.2.

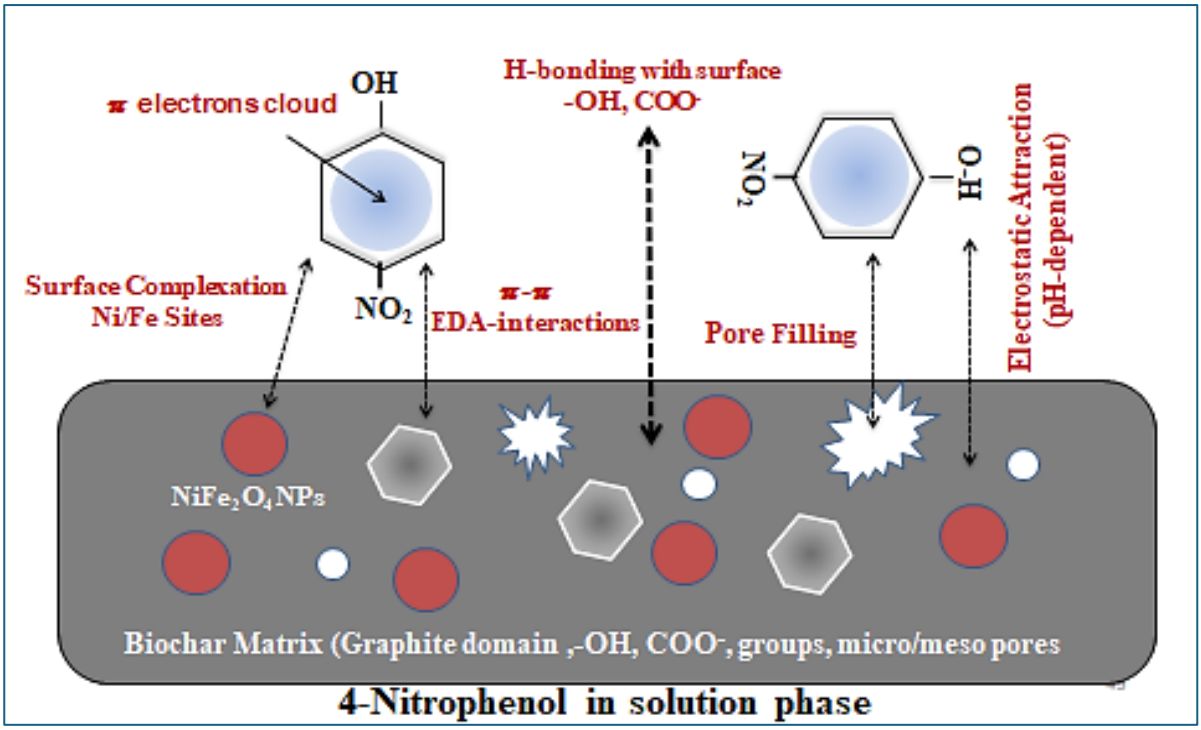


Figure 10 Proposed Mechanisms of 4-Nitrophenol Adsorption onto $NiFe_2O_4$/DSBC

Note. EDA = electron donor–acceptor. The schematic is conceptual and is not drawn to scale.

3.8 Reusability and Magnetic Recovery

Removal decreased from 92.0% in cycle one to 84.6% in cycle five (Table 6, Figure 11), a reduction of 7.4 percentage points that corresponds to retention of approximately 92.0% of the initial efficiency. The composite was separated from the solution within approximately 30 s using a hand-held magnet. Ni and Fe leaching into the treated water ranged from 0.012 to 0.024 mg/L and from 0.030 to 0.052 mg/L, respectively.

Table 6 Reusability and metal leaching over five adsorption–desorption cycles

Cycle	Removal (%)	Retained efficiency (%)	Ni leached (mg/L)	Fe leached (mg/L)
1	92.0	100.0	0.012	0.030
2	90.4	98.3	0.015	0.035
3	88.7	96.4	0.018	0.041
4	86.8	94.3	0.021	0.047
5	84.6	92.0	0.024	0.052

Note. Retained efficiency = (removal in cycle n / removal in cycle 1) × 100; percentages are rounded.

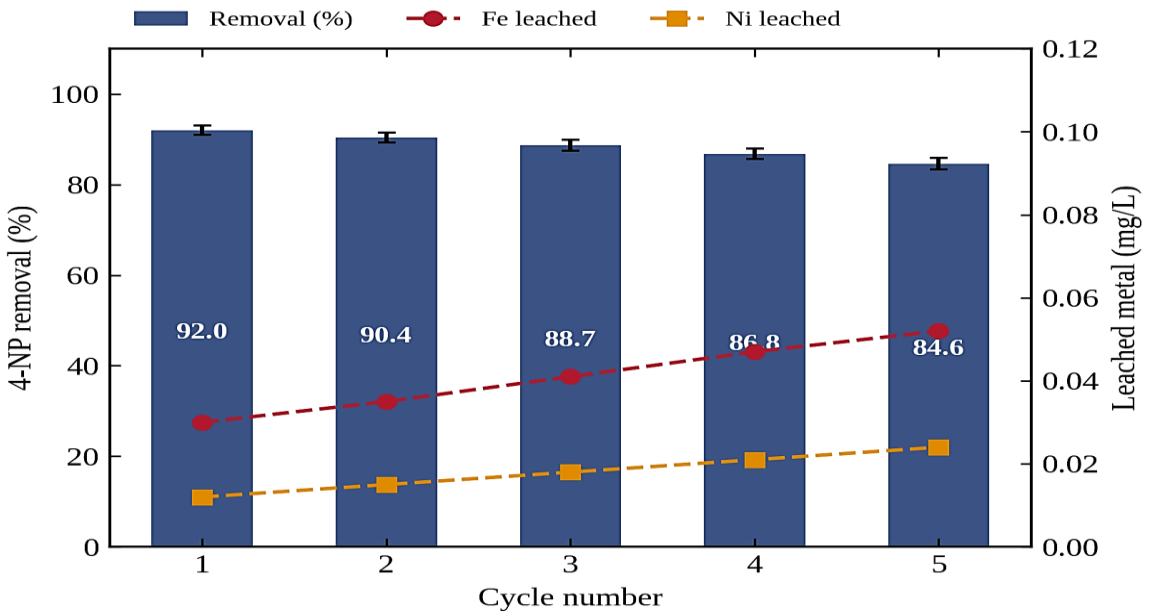


Figure 11 Reusability of $NiFe_2O_4$/DSBC Over Five Adsorption–Desorption Cycles

Note. Conditions: pH 5.0, dose 1.0 g/L, C_0 = 50 mg/L, 180 min, 298 K.

3.9 Structure–Property Relationships

The results of XRD, FTIR and SEM–EDX indicate that the ferrite phase is found on the biochar without breaking down the carbon framework. The broad carbon hump and the spinel reflections both appear in the composite pattern (Figure 2) and the Ni:Fe stoichiometry of 1:2.03 as determined by EDX is similar to that of the precursors (Section 2.3). In conjunction with the spinel reflections this favors the formation of $NiFe_2O_4$ instead of separate nickel and/or iron oxide phases. The crystallite size of the composite (21.4 nm; Table 2) is preventing the growth and coalescence of ferrite nuclei during co-precipitation and calcination on the biochar surface. An efficient way to well dispersed magnetic particles on biochar is to anchor ferrite particles on a porous carbon support [23].

The textural and magnetic data provide information about the primary structural characteristics and successful integration of the composite. The BET surface area (148.6 m^2/g) is larger than that of pure $NiFe_2O_4$ (≈57.0 m^2/g subject to synthesis conditions) [24], but much smaller than DSBC (215.3 m^2/g), and the saturation magnetization (8.67 emu/g) is lower than that typically reported for pure spinel nickel ferrite in literature) [25]. Both modifications are related to the close mass ratio of biochar to ferrite (about 1:1): Dilution of magnetic phase by non-magnetic carbon while part of biochar's pore network is blocked by the ferrite phase. The magnetization, however, was still adequate for separation using a hand-held magnet and a ratio between these parameters is reasonable. An increase in the ferrite loading would yield a greater magnetic response; however, it would be reasonable to assume it would decrease the amount of surface area even more.

As revealed by the pH profile (Figure 6a), the uptake is pH-dependent and depends on the surface charge of the nanocomposite (pHpzc = 6.4) and the pKa of 4-NP (pKa = 7.15) values. When pH is lower than both (pH<5.0), 4-NP is present as the neutral form, and the surface is positively charged, leading to the lack of electrostatic repulsion and making π–π electron donor–acceptor (EDA) and hydrogen-bonding interactions possible to operate in full swing. The decreasing above pH 7 is correlated with the formation of 4-nitrophenolate ion and a negative surface, as was reported with other carbon-based sorbents **[26]**. The lower removal at pH 2 (61.0%) is less favorable, which may be due to the competition of protons and 4-NP for surface sites.

Both the kinetic and isotherm results should be taken with caution. The initial rapid uptake and subsequent slow approach to equilibrium (Figure 8a) exhibited in porous adsorbents is typical of this

type of system and the pseudo-second-order model provided the best fit, (R^2 = 0.997; qe,cal = 46.7 mg/g and experimental = 46.0 mg/g). The good fit to this model alone does not prove chemisorption [27], but the non-linear Weber–Morris plot with a non-zero intercept (C = 11.2 mg/g) indicates that boundary-layer resistance and intraparticle diffusion are both involved. Similarly, the R^2 of the Langmuir model is 0.994–0.998, compared to the Freundlich model with R^2 of 0.961–0.973, indicating the formation of a monolayer on a relatively uniform surface, but the selection of the model based on linear regression can be misleading [19]. Thus, conclusions are made based on the agreement of multiple lines of evidence (kinetic, isotherm, thermodynamic, pH and FTIR) and are not solely based on a single fit.

The picture is supported by the thermodynamic data. The negative ΔG° values indicate spontaneous adsorption and the positive ΔH° values (18.5 kJ/mol) are in agreement with the increase in capacity from 85.0 to 99.0 mg/g of the product between 298 and 318 K. Such a value is typical of physical interactions, like hydrogen bonding, π–π stacking etc., rather than strong covalent bonds, and is consistent with the mechanism suggested in Figure 10. That is through π–π EDA interactions between the nitro-aromatic ring and the graphitic domains of the biochar, as well as hydrogen bonding with –OH and –COOH groups on the surface and hydroxylated Fe/Ni sites, pore filling in the mesopores (Table 2; mean pore diameter: 3.90 nm), and pH-dependent electrostatic effects. The contribution of each interaction has not been determined. It would require experiments with both DSBC and $NiFe_2O_4$ under the same conditions and surface analysis of the spent adsorbent by XPS.

Dalbergia sissoo materials have been primarily studied for dye removal such as wood dust for the removal of rhodamine B [9] and acid-activated leaf powder and magnetic iron oxide nanocomposite for the removal of alizarin red S [8]. In the present work, a biochar-supported ferrite is developed for a nitroaromatic pollutant, which is being extended to this feedstock. Another example of the use of a carbon support with spinel ferrite is in catalysis, and in this case Ni–$NiFe_2O_4$/carbon composites obtained from biomass were employed for hydrogenation [28], which will be a material class that can be recovered magnetically and used as an adsorbent. The reported capacities are sensitive to the feedstock and pyrolysis temperature; therefore, the same cannot be compared with different studies unless reported under identical conditions; pH and initial concentration (Ahmad et al., 2014; Mohan et al., 2014). Therefore, $NiFe_2O_4$/DSBC seems to be a promising, low cost candidate, because the maximum capacity of the material is 85.0 mg/g at 298 K and 99.0 mg/g at 318 K (compared to the limit of commercial activated carbon mentioned in the Introduction) with the additional advantage of magnetic separation.It is a locally plentiful waste stream that is valorized by using sawmill sawdust that is normally burnt or discarded.

Evaluating potential cyclic stability, the composite exhibited only a marginal decrease in removal efficiency of 7.4 percentage points over five successive cycles. This minor reduction could be due to incomplete desorption, pore blockage by 4-NP or loss of surface functional groups over time during the NaOH/ethanol regeneration. The loss of surface functional groups during the regeneration step was not quantified separately. The increase in the Ni and Fe release with the number of cycles indicates that a slight dissolution of the ferrite phase occurs. Since nickel is toxic, the leached concentration (0.012-0.024 mg/L) must be compared to the discharge and drinking-water limits that apply in the intended use. This short separation time of approximately 30 s is an operational benefit compared to filtration or settling of powdered biochar.

3.10 Comparison with Related Adsorbents

Work on D. sissoo-derived adsorbents has focused mainly on dyes, including activated carbon from wood dust for rhodamine B [9] and acid-activated leaf powder with its magnetic iron oxide composite for alizarin red S [8] The present study extends this feedstock to a biochar-supported ferrite for a nitroaromatic pollutant. Reported capacities depend on feedstock, pyrolysis conditions, pH and initial concentration [29], so comparisons across studies are only indicative. The review by El Messaoudi et al. (2024) [1] 4-NP capacities as high as 598 mg/g for a Ca–Al layered double hydroxide magnetic nanocomposite and 636 mg/g for magnetite nanoparticles; the capacities of $NiFe_2O_4$/DSBC (85.0 mg/g at 298 K and 99.0 mg/g at 318 K) are therefore moderate in absolute terms. Its appeal lies in the

use of a locally abundant waste feedstock combined with magnetic separation. A related biochar–$NiFe_2O_4$ composite removed ciprofloxacin with a maximum capacity of 68.79 mg/g [30] (Azzam et al., 2023) [30], but that value refers to a different pollutant and is not directly comparable. In order to quantify the superiority of the current study, the further detail comparative analysis is summarized in the table 7.

Table 7 Comparison of the adsorption capacity of $NiFe_2O_4$/DSBC for various pollutant removals with previously reported biochar supported metal based adsorbents.

Adsorbent / Nanocomposite	Biomass / carbon precursor	Important conditions	q_{max} (mg/g)	Ref:
Zn-NiF@PBC Nanocomposite	pinecone	pH 3 ; 0.25 g ; 75 mg/L ; 80 min	45.6	[31]
BC-NiS	Banana Peel waste	pH 6; 25°C	41.66	[32]
GT-BC@nZVI/Cu	Peanut shell + green tea	pH 5; 313 K; 30 min	35.21	[33]
BC-NiFe2O4	Banana Peel	pH 6; 25°C; 100 mg adsorbent;	68.7	[30]
Fe3O4/biochar	poplar wood	25 °C; 30 min,; pH 7	73.4	[34]
BFS-supported Biochar Composite	Sewage sludge + wood sawdust + BFS	pH 6; 25 °C; 20 mg/L; 1 g/L; 90 min	12	[35]
Nanobiochar	Pomegranate peel	pH 6; 298 K; 15 mg/30 mL	84.75	[36]
Chitosan/biochar hydrogel beads (CBHB)	Yuzu marc wastes	pH 3.0; 30°C, 48h	34.90	[37]
Humic acid coated magnetic biochar	Potato stems and leaves	pH 5.0 – 6.0; dose 0.2 – 0.4 g/L; 24 h; 15 °C	8.68	[38]
$NiFe_2O_4$/DSBC Nanocomposite	Dalbergia sissoo sawdust	pH 5; 298 K; 50 mg/L; 1.0 g/L	85.0	This Study

4. Conclusions

The $NiFe_2O_4$/DSBC nanocomposite was prepared by co-precipitation of nickel ferrite on biochar from Dalbergia sissoo sawdust. It is a mesoporous material (148.6 m^2/g) with a cubic spinel structure (crystallite size 21.4 nm) and a saturation magnetization of 8.67 emu/g, which is sufficient for rapid separation with a hand-held magnet. At pH 5.0, 1.0 g/L, 50 mg/L and 298 K, the composite removed 92.0% of 4-NP.

Adsorption followed pseudo-second-order kinetics and the Langmuir isotherm, with a maximum capacity of 85.0 mg/g at 298 K that increased to 99.0 mg/g at 318 K. The process was spontaneous and endothermic. The proposed mechanism combines π–π EDA interactions, hydrogen bonding, pore filling and pH-dependent electrostatic effects. After five adsorption–desorption cycles the composite retained 92.0% of its initial efficiency, with low Ni and Fe leaching, which supports its reuse.

$NiFe_2O_4$/DSBC is therefore a promising, low-cost and magnetically recoverable adsorbent for 4-nitrophenol. Tests in real effluents and in continuous-flow systems are the next step.

REFERENCES

1. El Messaoudi, N., et al., *A comprehensive review on designing nanocomposite adsorbents for efficient removal of 4-nitrophenol from water.* Nano-Structures & Nano-Objects, 2024. **40**: p. 101326.
2. Hu, Q. and L. Hao, *Adsorption Technologies in Wastewater Treatment Processes.* Water, 2025. **17**(15): p. 2335.
3. Varkolu, M., et al., *Recent Advances in Biochar Production, Characterization, and Environmental Applications.* Catalysts, 2025. **15**(3): p. 243.
4. Du, L., et al., *Evolution of Biochar Structure and Its Impact on Volatile Adsorption and Reforming during Char-Recycled Pyrolysis.* Energy Material Advances, 2025. **6**.
5. Li, P., et al., *Biochar Innovations for Organic Pollutant Remediation in Contaminated Soils.* Molecules, 2026. **31**(3).
6. Gęca, M., M. Wiśniewska, and P. Nowicki, *Biochars and activated carbons as adsorbents of inorganic and organic compounds from multicomponent systems - A review.* Advances in colloid and interface science, 2022. **305**: p. 102687.
7. Sweed, A., et al., *impact of pyrolysis temperature and feedstock type on biochar's chemical properties and adsorption efficiency of lead and cadmium from aqueous solutions.* Menoufia Journal of Soil Science, 2026. **11**: p. 147-160.
8. Nawaz, S., et al., *Kinetics and thermodynamics investigations of efficient and eco-friendly removal of alizarin red S from water via acid-activated Dalbergia sissoo leaf powder and its magnetic iron oxide nanocomposite.* Frontiers in Chemistry, 2024. **Volume 12 - 2024**.
9. Shrestha, D., *Efficiency of Wood-Dust of Dalbergia sisoo as Low-Cost Adsorbent for Rhodamine-B Dye Removal.* Nanomaterials, 2021. **11**(9): p. 2217.
10. Santhosh, C., et al., *Synthesis and characterization of magnetic biochar adsorbents for the removal of Cr(VI) and Acid orange 7 dye from aqueous solution.* Environ Sci Pollut Res Int, 2020. **27**(26): p. 32874-32887.
11. Nan, L., et al., *Application of Magnetic Aquatic Plant Biochar for Efficient Removal of Antimony from Water: Adsorption Properties and Mechanism.* Separations, 2025. **12**(1): p. 2.
12. Fröhlich, A.C., E. Foletto, and G. Dotto, *Preparation and characterization of NiFe2O4/activated carbon composite as potential magnetic adsorbent for removal of ibuprofen and ketoprofen pharmaceuticals from aqueous solutions.* Journal of Cleaner Production, 2019. **229**.
13. Brunauer, S., P.H. Emmett, and E. Teller, *Adsorption of Gases in Multimolecular Layers.* Journal of the American Chemical Society, 1938. **60**(2): p. 309-319.
14. Thommes, M., et al., *Physisorption of gases, with special reference to the evaluation of surface area and pore size distribution (IUPAC Technical Report).* Pure and Applied Chemistry, 2015. **87**(9-10): p. 1051-1069.
15. Lagergren, S., *Zur theorie der sogenannten adsorption geloster stoffe.* 1898.
16. Ho, Y.S. and G. McKay, *Pseudo-second order model for sorption processes.* Process Biochemistry, 1999. **34**(5): p. 451-465.
17. Weber Walter, J. and J.C. Morris, *Kinetics of Adsorption on Carbon from Solution.* Journal of the Sanitary Engineering Division, 1963. **89**(2): p. 31-59.
18. Langmuir, I., *THE ADSORPTION OF GASES ON PLANE SURFACES OF GLASS, MICA AND PLATINUM.* Journal of the American Chemical Society, 1918. **40**(9): p. 1361-1403.

19. Tran, H.N., et al., *Mistakes and inconsistencies regarding adsorption of contaminants from aqueous solutions: A critical review.* Water Research, 2017. **120**: p. 88-116.
20. Wang, J. and X. Guo, *Adsorption kinetic models: Physical meanings, applications, and solving methods.* Journal of Hazardous Materials, 2020. **390**: p. 122156.
21. Nguyen, D., *Enhanced Adsorptive Removal of 4-Nitrophenol, Methylene Blue, and Tetracycline using a NiFe2O4/AC Composite.* Water, Air, & Soil Pollution, 2026. **237**.
22. Duan, S., et al., *Characteristics of digested sludge-derived biochar for promoting methane production during anaerobic digestion of waste activated sludge.* Bioresource Technology, 2023. **384**: p. 129245.
23. Nguyen, D.T.C., *Magnesium ferrite-based composites for water treatment: synthesis strategies, adsorption performance, modelling and regeneration.* Nanoscale Advances, 2026. **8**(18): p. 4989-5015.
24. Hariharasuthan, R., et al., *Characterization of NiFe2O4 (Nickel Ferrite) nanoparticles with very low magnetic saturation synthesized via co-precipitation method.* Applied Physics A, 2022. **128**(12): p. 1045.
25. Wen, J., et al., *Synthesis and magnetic properties of spinel NiFe2O4 nanoparticles by oxidation roasting technique.* Materials Science and Engineering: B, 2025. **319**: p. 118375.
26. Ahmed, M.A., M.A. Ahmed, and A.A. Mohamed, *Removal of 4-nitrophenol and indigo carmine dye from wastewaters by magnetic copper ferrite nanoparticles: Kinetic, thermodynamic and mechanistic insights.* Journal of Saudi Chemical Society, 2023. **27**(6): p. 101748.
27. Wang, J. and X. Guo, *Adsorption isotherm models: Classification, physical meaning, application and solving method.* Chemosphere, 2020. **258**: p. 127279.
28. Liu, W.-J., K. Tian, and H. Jiang, *One-pot synthesis of Ni–NiFe2O4/carbon nanofiber composites from biomass for selective hydrogenation of aromatic nitro compounds.* Green Chemistry, 2015. **17**(2): p. 821-826.
29. Qiu, M., et al., *Biochar for the removal of contaminants from soil and water: a review.* Biochar, 2022. **4**(1): p. 19.
30. Azzam, A.B., et al., *Heterogeneous porous biochar-supported nano NiFe(2)O(4) for efficient removal of hazardous antibiotic from pharmaceutical wastewater.* Environ Sci Pollut Res Int, 2023. **30**(56): p. 119473-119490.
31. Masuku, M., et al., *Advancing the development of nanocomposite adsorbent through zinc-doped nickel ferrite-pinecone biochar for removal of chromium (VI) from wastewater.* Science of The Total Environment, 2024. **908**: p. 168136.
32. Azzam, A.B., et al., *Construction of porous biochar decorated with NiS for the removal of ciprofloxacin antibiotic from pharmaceutical wastewaters.* Journal of Water Process Engineering, 2022. **49**: p. 103006.
33. Li, T., et al., *Simultaneous removal of p-nitrophenol and Cr(VI) using biochar supported green synthetic nano zero valent iron-copper: Mechanistic insights and toxicity evaluation.* Process Safety and Environmental Protection, 2022. **167**: p. 629-640.
34. Zhang, X., et al., *An achieved strategy for magnetic biochar for removal of tetracyclines and fluoroquinolones: Adsorption and mechanism studies.* Bioresource Technology, 2023. **369**: p. 128440.
35. Rangappa, H.S., et al., *Industrial waste-derived biochar composites for the removal of water-borne 4-nitrophenol: assessing cost-effectiveness and sustainability.* Environmental Science and Pollution Research, 2025. **32**(39): p. 22544-22559.

36. Kustomo and S.F. Yau Li, *Nanobiochar from pomegranate peel biomass for enhanced 4-nitrophenol removal: synthesis, characterization, and performance evaluation.* Environmental Nanotechnology, Monitoring & Management, 2026. **25**: p. 101123.
37. Afzal, M.Z., et al., *Enhancement of ciprofloxacin sorption on chitosan/biochar hydrogel beads.* Science of The Total Environment, 2018. **639**: p. 560-569.
38. Zhao, J., et al., *Coating magnetic biochar with humic acid for high efficient removal of fluoroquinolone antibiotics in water.* Science of The Total Environment, 2019. **688**: p. 1205-1215.

Acknowledgements
The authors acknowledged the anonymous reviewers for comments to improve the quality of this work.

Authors and Affiliations
Author
1. Muhammad Imran (First Author and Corresponding authors),
Department of Chemistry, M.A. Kazi Institute of Chemistry,
University of Sindh, Jamshoro, Province of Sindh, Pakistan.
Email: imrankhattak024@gmail.com

Co-Authors
2. Prof': Dr Humaira Khan (Second Author (Supervisor) and Senior Corresponding authors),
Department of Chemistry, M.A. Kazi Institute of Chemistry,
University of Sindh, Jamshoro, Province of Sindh, Pakistan.
Email: humairasadq@gmail.com

3. Dr Aamna Balouch (Third Author (Co-Supervisor)
National Centre of Excellence in Analytical Chemistry,
University of Sindh, Jamshoro, Province of Sindh, Pakistan.
Email: aamna_balouch@yahoo.com

4. Farooq Azam Khatri
Department of Chemistry, M.A. Kazi Institute of Chemistry,
University of Sindh, Jamshoro, Province of Sindh, Pakistan.
Email fazamkhatri@gmail.com

Corresponding authors
Correspondence to Muhammad Imran and Dr Humaira Khan

Ethics declarations

Competing interests
The authors disclaim any financial conflicts of interest.